[15] R. F. Milsom, N.H.C. Reilly, and M. Redwood, "Analysis of generation and detection of surface and bulk acoustic waves by interdigital transducers," *IEEE Trans. Sonics Ultrason.*, vol. SU-24, pp. 147-166, 1977.
[16] C. A. Greebe, P. A. Van Dalen, T. J. Swanenburg, and J. Wolter, "Electric coupling properties of acoustic and electric surface waves," *Phys. Rep.*, vol. 1C, pp. 235-268, 1971.
[17] R. A. Sykes, "Modes of motion in quartz crystals," *Bell Syst. Tech. J.*, vol. 23, p. 52, 1944.
[18] G. W. Farnell, "Symmetry considerations for elastic layer modes propagating in anisotropic piezoelectric crystals," *IEEE Trans. Sonics Ultrason.*, vol. SU-17, pp. 229-237, 1970.
[19] D. L. Lee, "Analysis of energy trapping effects for *SH*-type waves on rotated *Y*-cut quartz," *IEEE Trans. Sonics Ultrason.*, vol. SU-28, pp. 330-341, 1981.

Fabien Josse (S'78-M'82) was born in Porto-Novo, Benin, on December 22, 1951. He received the Licence de Mathematique et Physique from the Universite National du Benin in 1976, the M.S. and Ph.D. degrees in electrical engineering from the University of Maine at Orono in 1979 and 1982, respectively.

He joined the faculty of the Department of Electrical Engineering and Computer Science at Marquette University, Milwaukee, WI, in 1982, where he is investigating reflected bulk waves for microwave acoustic and acoustoelectric device applications. His current research interests also include signal analysis and processing in optical fiber systems.

Dr. Josse is a member of Eta Kappa Nu and Sigma Xi.

Residual Bulk Mode Levels in (*YXl*)128° $LiNbO_3$

ROBERT S. WAGERS, FELLOW, IEEE, ROBERT W. COHN, MEMBER, IEEE

Abstract—**Bulk mode energy transport between interdigital transducers on a parallelopiped of (*YXl*)128°$LiNbO_3$ is examined. The several types of energy transport, and their trajectories, are delineated and quantified. Their contributions to the terminal properties (S_{21}) of the filter are analyzed in both the time and frequency domains. A waveform processing procedure is described which can reduce, or in some cases eliminate, the contributions made by bulk modes to the S_{21} data of SAW filters.**

I. Introduction

In surface acoustic wave (SAW) filters, the interdigital transducer (IDT) launches and detects surface waves. The IDT is an effective radiator of other acoustic modes as well. In the literature, bulk mode [1] and plate mode [2] analyses have been used with equal success in describing these spurious modes. The choice of one representation or the other is based on considerations of substrate geometry, frequency range of applicability, and desired accuracy. For relatively wide-band devices the ray tracing techniques applicable to bulk wave analysis have been shown to be accurate and thus are commonly used.

A bulk wave launched by the IDT carries energy from the input to the output of the SAW filter. This energy transport tends to occur at all frequencies from the center of the SAW filter response to frequencies well above the SAW response. Because SAW filters are typically designed for bandpass shaping associated with SAW energy transport only, the energy carried by the bulk waves degrades the performance of SAW filters. This is most serious on the high-frequency side of SAW filters where the bulk wave energy may exceed the limits for out-of-band rejection of the filter.

A great deal of effort has been directed at finding new cuts of crystalline materials in which the bulk mode excitation is minimized. One of these cuts that has come into popular use is the 128° rotated *Y*-cut of $LiNbO_3$. In [3]-[6] it is shown that superior spurious mode properties are exhibited by the cut. However, (*YXl*)128°$LiNbO_3$ does have residual spurious modes, and achievement of low spurious levels over large bandwidths is dependent on effective backside treatment of the crystal.

In a continuing effort to define the controlling processes in SAW transduction [7], we have attempted to measure the SAW filter response associated with the Rayleigh mode alone. For these measurements we chose the (*YXl*)128°$LiNbO_3$ cut to minimize bulk and plate mode interference. However, even this cut of $LiNbO_3$ does not provide sufficiently uncorrupted Rayleigh mode data. As a consequence we have delineated the nature of the residual bulk mode levels in the (*YXl*)128°$LiNbO_3$ cut and defined means for removing their influence from the terminal measurements of SAW filters.

II. (*YXl*)128°$LiNbO_3$ Bulk Modes

Fig. 1 illustrates the $LiNbO_3$ crystal and interdigital transducers thereon employed in this study. Both transducers employ double electrodes; one transducer is a 3-finger-pair unapodized IDT, and the other transducer is a 10-finger-pair apodized IDT with a Dolph-Tchebysheff weighting (Taylor approximation, $n = 5$, 37 dB sidelobe level [8]). The SAW filter was designed to operate at 150 MHz with a center frequency wavelength of 25.81 μm. The substrate was slightly

Manuscript received April 2, 1984; revised May 21, 1984.
The authors are with Central Research Laboratories, Texas Instruments Inc., Dallas, TX 75265.

0018-9537/84/0500-0168$01.00

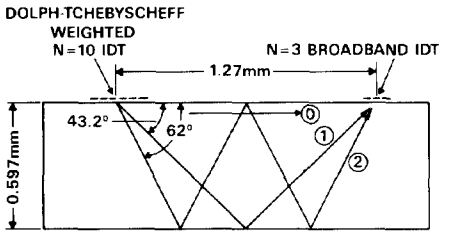

Fig. 1. SAW filter IDT and $(YXl)128°LiNbO_3$ substrate configuration. An IDT periodicity of 25.81 μm yielded a center frequency of 150 MHz. Overlaps in the apodized IDT varied from 9.9 λ_0 to 67.9 λ_0.

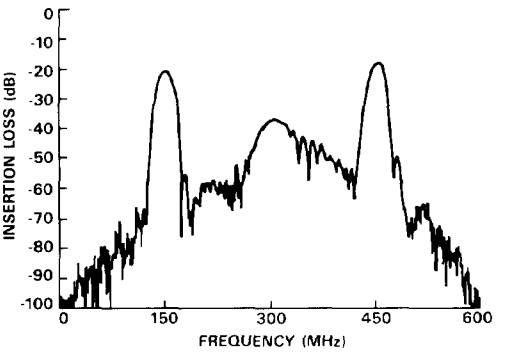

Fig. 2. Total acoustic response of the SAW filter. Both SAW and bulk wave energy are present. Electromagnetic feedthrough was eliminated from response by Fourier transformation and windowing operations.

over 20 wavelengths thick, and the distance between the centers of the transducers was 49.2 wavelengths.

Shown in Fig. 1 are three possible paths for bulk acoustic signals to follow in going from the input transducer to the output transducer. Path 0 represents direct transmission along the surface of the crystal and is the path followed by SAW and on-axis bulk waves. Path 1 includes one bounce off the bottom of the crystal by bulk waves. Path 2 includes two bounces off the backside of the crystal by bulk waves. This geometry will be used to interpret the bulk mode properties of the filter.

Fig. 2 shows the total acoustic response of the SAW filter. At 150 MHz is the strong SAW filter response with an insertion loss of 21 dB. At 450 MHz is the third harmonic SAW response. These two responses are relatively narrow-band; 50 MHz away from the center frequency of the passband the Rayleigh response should be at the -85 dB level of Fig. 2. All other signals shown in Fig. 2 are bulk wave responses of the crystal. At 300 MHz the insertion loss due to bulk mode energy is only 16 dB less than the SAW response at 150 MHz. These results were obtained from crystals with the configuration of Fig. 1; the backside of the crystals had not been treated in any respect. Note in Fig. 2 that the first high-frequency sidelobe of the SAW response occurs 20 percent higher in frequency than the midband of the fundamental Rayleigh response. At that frequency the untreated crystal manifests bulk responses only 15 dB below the first high-frequency sidelobe of the SAW response. These levels can be contrasted with those evident in the photographs of [3]. The levels they reported at the center of the band for residual bulk mode levels in a crystal that had the backside treated were ~65 dB down from the peak SAW response, whereas those evident in Fig. 2 are only ~50 dB down (based on extrapolation of the out-of-band bulk mode levels into the passband or consideration of Fig. 5 to be explained below).

Substantial backside treatment of the crystals was performed on these filters in order to reduce the bulk mode distortion of the high-frequency sidelobes. We found that neither the on-axis bulk modes (main passband) not the bulk modes in the vicinity of the high-frequency sidelobes were removed as cleanly as required. The inability to reduce the bulk modes within the SAW passband to the levels of [3] is possibly due to the smaller overlaps in these filters [9]. Whereas the filter in [3] employed an unapodized transducer with a 52.5 wavelength wide aperture, our IDT was apodized from 67.9 wavelength wide down to a minimum overlap of 9.9 wavelengths.

In the following sections we detail the physical nature of the spurious bulk modes of $(YXl)128°LiNbO_3$. We will show the propagation mechanics for the several acoustic modes and also illustrate the relative levels of each of the modes present in the filter. Finally a technique will be presented for processing the S_{21} data of the filters to substantially reduce the contributions that arise due to bulk modes.

III. Experimental Procedure

SAW filters of the type shown in Fig. 1 had their entire top surface coated with Apiezon W wax (black wax). The black wax was applied to absorb all SAW energy from the crystal. Bulk wave transmission from input to output transducer is also affected by the application of black wax but to a very much smaller degree [2], [10]. Bulk mode amplitudes are only attenuated ~1 dB, whereas surface wave energy can be attenuated 60 to 70 dB depending upon the propagation length through the black wax. Fig. 3 shows the frequency domain data for one of these filters after the black wax had been applied. (In obtaining Fig. 3, Fourier transformation and windowing operations were performed to eliminate electromagnetic feed-through.) Note from Fig. 2 that the SAW insertion loss is 21 dB; thus, in Fig. 3 one can see that the spurious level of transmission is only 45 dB below the SAW response at 150 MHz; it rises to even higher levels at higher frequencies.

Fig. 4 shows the impulse response of one of the black-waxed SAW filters. All of the time shown along the abscissa of Fig. 4 represents positive time for this causal filter. The rise in the trace at the right-hand side of Fig. 4 occurs at the end of the of the fast Fourier transform (FFT) cell. This rise is a consequence of windowing in the frequency domain to the first 600 MHz. Attendant with frequency domain windowing is a time domain convolution with a narrow sinc-like function which spreads the electromagnetic feedthrough delta function at $t = 0$ to $t > 0$ and $t < 0$. The $t < 0$ portion intrudes at the upper end of the time window where the waveform begins its repetition [11].

Five distinct peaks stand out in the impulse response in Fig. 4. There is a response at $t = 0$, corresponding to the crosstalk, and four time-resolved acoustic responses with time delays from 194 ns to 423 ns. For comparison note that the Rayleigh wave response would have occurred at a time delay of 330 ns. The response at 320 ns of Fig. 4 is composed of two physically distinct processes. Labels identifying each of these modes appear in Figs. 4 and 5. Summary data and the labels for these modes are given in Table I.

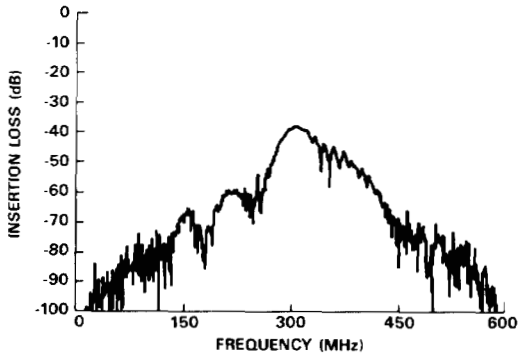

Fig. 3. Insertion loss characteristics of black-waxed filter. SAW response is absent due to black wax. Electromagnetic feedthrough was eliminated from response by Fourier transformation and windowing operations.

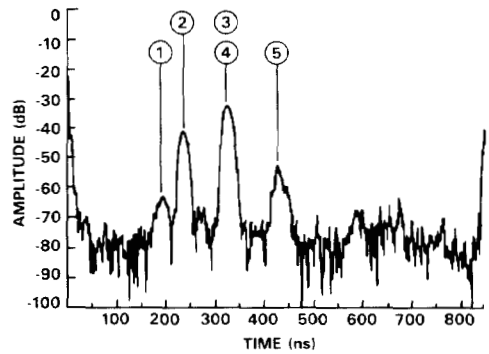

Fig. 4. Fourier transform of frequency response comprised of the Fig. 3 frequency response and electromagnetic feedthrough. Response at $t = 0$ is electromagnetic feedthrough. Other four peaks are acoustic signals designated by mode index (I).

To understand how each of the four acoustic peaks contributed to the overall frequency response of the black-waxed filter, each of the peaks was separately fast Fourier transformed to the frequency domain. These responses are shown in Fig. 5. Fig. 5(a) shows the frequency response of the pulse from Fig. 4 which occurs at 194 ns. It has a center frequency of 255 MHz. The bandwidth of this response is such that the signal does not extend into the Rayleigh wave response to a significant degree. The level of acoustic activity of this bulk mode in the vicinity of the sidelobes of the SAW response is -84 dB. In Fig. 5(b), the response centered at 362 MHz corresponds to the time domain peak at 233 ns. This response is much broader than the SAW response; however, it does not extend into the frequency range of the SAW response at significant levels.

The time domain response at 320 ns has two major responses in the frequency domain; these are shown in Fig. 5(c). The largest is centered at 303 MHz and does not extend into the range of the SAW response. The second one is centered at 153 MHz and is thus directly in the passband of the SAW filter response. The bulk wave response in the SAW passband is only 48 dB below the peak of the SAW response.

Finally, the time domain response at 423 ns has a frequency domain representation as shown in Fig. 5(d). This response peaks at 218 MHz. It is responsible for most of the bulk wave interference appearing immediately to the high side of the SAW passband. An overlay of Fig. 2 and Fig. 5(d) shows that

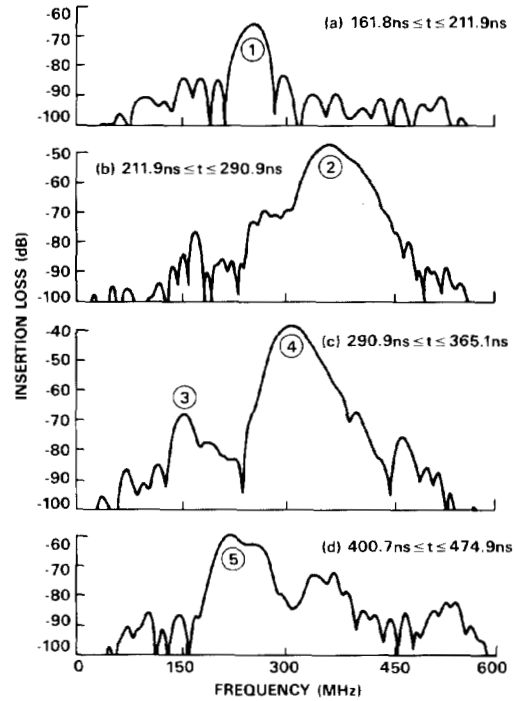

Fig. 5. Fourier transforms of portions of the acoustic response of Fig. 4. Time domain data was nulled everywhere except in regions specified on each plot before taking the transform.

TABLE I
MEASURED TIME AND FREQUENCY DOMAIN DATA FOR THE TERMINAL RESPONSE OF SAW FILTERS OF THE TYPE ILLUSTRATED IN FIG. 1

TIME DELAY (ns)	FREQUENCY (MHz)	MODE
0	All	EM Crosstalk
194	255	Bulk (1)
233	362	Bulk (2)
320	153, 303	Bulk (3), (4)
423	218	Bulk (5)
330	151	Rayleigh

the bulk wave responses between the first high-frequency sidelobe of the SAW filter and 250 MHz are almost entirely composed of the Fig. 5(d) frequency response.

The shoulder near the high-frequency side of mode 3 in Fig. 5(c) is ~24 dB down from the first sidelobe of the SAW filter and only 10 dB down from the second sidelobe of the SAW filter. This signal (174 MHz $\leqslant f \leqslant$ 235 MHz) is an artifact of the measurements and signal processing. A number of other minor peaks also appear in Fig. 5(a)-(d). However their levels are sufficiently close to the total "noise" level that they could not be unequivocally associated with a distinct mode of acoustic energy transport. Accordingly, only the major peaks have been labeled.

IV. Analysis: Single Mode Transport

Most of the bulk mode responses illustrated in Fig. 5 and summarized in Table I can be explained with reference to Figs. 1 and 6. Fig. 1 shows three methods of energy transport from input to output. In traveling Path 0 the wave does not bounce off the backside of the crystal. Path 1 has one bounce off the backside of the crystal, and Path 2 includes two bounces off the backside of the crystal. If a wave travels Paths 1 or 2

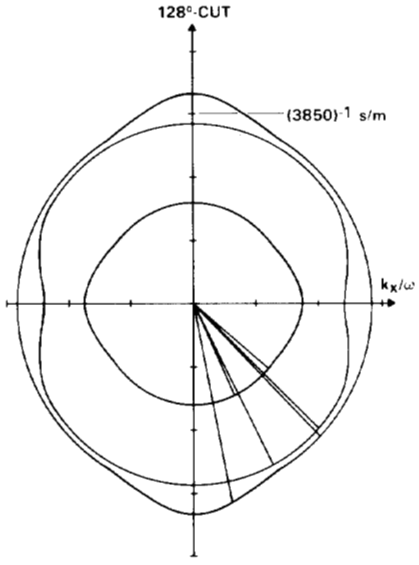

Fig. 6. Inverse velocity curves of $(YXl)128^{\circ}LiNbO_3$. Upper three solid rays terminating on inverse velocity branches define modes having group velocities of 42.3°. Lower three rays terminate on branches at positions having group velocity angles of 62° downward from the x axis.

TABLE II
DATA FROM INVERSE VELOCITY CURVES OF FIG. 6 FOR SLOW SHEAR (SS), FAST SHEAR (FS), AND LONGITUDINAL (L) WAVES PROPAGATING ALONG PATHS (0), (1), AND (2) SHOWN IN FIG. 1 (DATA GIVEN ARE PHASE AND GROUP VELOCITY ANGLES, PHASE AND GROUP VELOCITIES, TIME DELAY, AND FREQUENCY OF OPERATION FOR FIG. 1 FILTER)

Branch	θ_p (Degrees)	θ_g (Degrees)	V_p (m/s)	V_g (m/s)	T(ns)	F(MHz)	Path	Mode
SS	0	0	4063	4063	313	157	0	(3)
FS1	19.6	0	4397	4668	272	181	0	
FS2	0	0	4795	4795	265	186	0	
L	0	0	6628	6628	192	257	0	(1)
SS	45.0	43.2	4010	4012	434	220	1	(5)
FS	44.3	43.2	4064	4065	429	220	1	
L	41.5	43.2	7391	7395	236	382	1	(2)
SS	79.2	62.0	3601	3770	718	745	2	
FS	63.3	62.0	4040	4041	669	348	2	
L	65.3	62.0	7268	7281	372	674	2	

it would have to be launched from the input transducer at group velocity angles of 43.2° or 62°, respectively.

Fig. 6 shows the inverse velocity curves for $(YXl)128^{\circ}$-$LiNbO_3$. Shown on the plots are two groups of rays which terminate on the three inverse velocity curves. In the upper group of 3, each mode has a group velocity angle of 42.3°. In the lower group of 3, each has a group velocity angle of 62°. From the curves in Fig. 6, the phase and group velocities, and their angles, can be all be measured or calculated. These data are shown in Table II. By using the path length for each of the three possible paths and the requirement that the wavelength of the bulk mode be phase matched to the IDT, the time delay and the center frequency of operation associated with each mode for each path can be calculated. These data are also shown in Table II.

Comparing the experimental results of Table I with the allowed time delays and frequencies of Table II, we are able to identify most of the experimentally observed modes. Response number 1 is a longitudinal mode traveling directly from the input transducer to the output transducer. Response number 2 is a longitudinal mode executing one bounce from the bottom side of the crystal. Response number 3 is a slow shear mode traveling directly from the input IDT to the output IDT. Response number 4 cannot be explained on the basis of a direct one bounce or two bounce trajectory; it will be explained in the next section. Finally, response number 5 could be attributed to the slow shear and/or the fast shear executing one bounce from the bottom side of the crystal. We know from other calculations, though, that the slow shear coupling to the IDT is at least 12 dB larger than that of the fast shear coupling so mode 5 is attributed to the slow shear branch. Also it is noted that none of the modes is a consequence of two bounces off the backside of the crystal.

V. ANALYSIS: TRANSPORT BY MODE CONVERSION

Response number 4 in Table I cannot be described by a simple trajectory from the input IDT to the output IDT. As shown in Table II all three of the paths of Fig. 1 have time and frequency parameters associated with them that are sufficiently different from mode 4 of Table I that the difference between the theoretical and experimental data could not be attributed to experimental error. Instead, response number 4 arises from a trajectory as illustrated in Fig. 7. The input IDT launches a slow shear wave with a group velocity angle of 52.3° downward from the surface of the crystal. At the bottom side of crystal, the slow shear wave mode converts to a longitudinal wave which travels upward at an angle of 36.4° to reach the output IDT. The modes involved in this energy transport are illustrated on the inverse velocity plot of Fig. 8.

Fig. 8 shows a coupling of the outer shear mode and the inner longitudinal wave. For mode conversion to occur between these two modes they must have the same phase velocity along the x axis; thus, the dashed vertical line passes through the active modes. The group velocity directions for the two modes are represented as arrows which are normal to the inverse velocity curves. Note that the inverse velocity curves are relatively flat at the points indicated by the dashed vertical line. Thus, for a wide band of frequencies the trajectories vary little from the nominal values of 52.3° and 36.4°. Therefore, this mode of energy transport should be relatively broad-band. Fig. 5(c) clearly shows that the response which is centered at 303 MHz has an extremely broad response.

Table III shows data taken from Fig. 8 which represents the phase and group velocity angles, the phase and group velocities, time delays of the two legs of the total path from input to output, and the frequency of synchronous operation of the IDT for modes traveling the two paths. In Table III, X represents the horizontal distance between the IDT's that a wave travels from an IDT to the position above the reflection point on the backside of the crystal. Thus, the sum of these two X values should add to 1.27 mm (the center-to-center distance between IDT's). Note that the total time delay and frequency

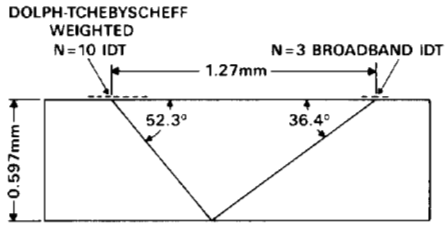

Fig. 7. Path traveled by the acoustic modes that produced response at $t = 320$ ns and $f = 303$ MHz.

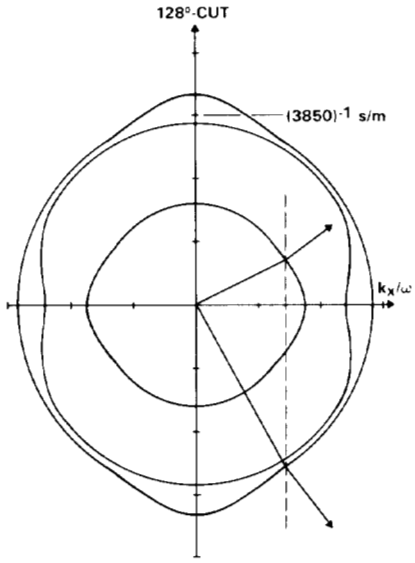

Fig. 8. Inverse velocity curves of $(YXl)128°LiNbO_3$. Dashed line intersects longitudinal and shear wave branches at points having same x-axis component of the velocity. Arrows normal to inverse velocity curves illustrate group velocity directions of 52.3° downward and 36.4° upward.

TABLE III
DATA FROM INVERSE VELOCITY CURVES OF FIG. 8 FOR MODE CONVERSION BETWEEN A SLOW SHEAR WAVE AND A LONGITUDINAL WAVE (X REPRESENTS HORIZONTAL DISTANCE FROM AN IDT TO THE POSITION ABOVE REFLECTION POINT ON BACKSIDE OF CRYSTAL)

	θ_p (Degrees)	θ_g (Degrees)	V_p (m/s)	V_g (m/s)	T(ns)	F(MHz)	X(mm)
Shear	60.5	52.3	3943	3984	189	310	0.461
Longitudinal	26.1	36.4	7182	7299	138	310	0.809
TOTAL					327		1.271

found in Table III agree to within 2.5 percent of the experimental results illustrated for mode 4 in Table I.

Two paths of the type illustrated in Fig. 7 are possible between the input and output IDT's. The path illustrated in Fig. 7 slopes downward from the left-hand transducer at 52.3° and upward to the output transducer at 36.4°. An equally allowed possibility is downward from the left-hand transducer at 36.4° and upward to the output transducer at 52.3°. Both paths are active during device operation.

VI. SANDBLASTING RESULTS

These devices had their lower surfaces sandblasted to eliminate as much of the bulk mode content as possible. The spurious frequency response of a black-waxed sandblasted device

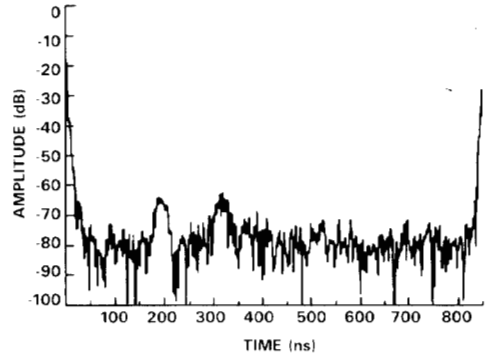

Fig. 9. Time domain response of black-waxed sandblasted SAW filter of type illustrated in Fig. 1.

was transformed to the time domain; a typical impulse response is shown in Fig. 9. The device exhibits a crosstalk response, which occurs at $T = 0$, and two acoustic responses. The acoustic response at 194 ns was not altered by the sandblast operation. It occurs at exactly the same time delay as it did in Fig. 4 and with approximately the same insertion loss of 64 dB. The time domain response at 233 ns in Fig. 5 is seen to be completely absent in Fig. 9 after sandblasting. This response was associated with mode 2 from Table I. Mode 2, the longitudinal mode which executed one bounce from the bottom of the crystal, is thus totally absent from the time domain response of Fig. 9 after backside sandblasting.

There is a time domain response at 313 ns in Fig. 9. This is essentially coincident with the time domain response shown in Fig. 4 which was centered at 320 ns. Recall that the response of Fig. 4 at 320 ns was associated with two acoustic responses with center frequencies of 153 MHz and 303 MHz. The 303 MHz response is the wave which undergoes mode conversion. It is the stronger of the two responses, being some 30 dB larger than the response at 153 MHz. The smaller response at 153 MHz was associated with direct transmission of a slow shear wave along the crystal surface and thus, should not have been affected by sandblasting at all. It is interesting to note that the time domain response shown at 313 ns in Fig. 9 is ~30 dB lower than the time domain response shown at 320 ns in Fig. 4. Thus, the results for the sandblasted crystal are physically consistent with all of the observed levels and the physical explanations for the two modes of transport. Finally, note that Fig. 4 shows an impulse response at 423 ns that is totally absent from the Fig. 9 impulse response. This is physically consistent with the explanation put forth for the mode with 423 ns delay. This mode would have been removed by sandblasting since the shear wave is reflected from the backside of the crystal.

Fig. 10 shows the Fourier transforms associated with the two time-domain acoustic responses of Fig. 9. The time domain response at 194 ns has a peak frequency domain response (Fig. 10) at 255 MHz. Reference to Table I shows that this set of numbers is essentially equal to the on-axis longitudinal wave information for the device without sandblasting. The time domain response at 313 ns in Fig. 9 has a peak response in the frequency domain (Fig. 10) at 150 MHz. Reference to Table I shows that this was associated with mode 3 of the unsandblasted device. That mode was found to be the slow shear mode propagating on-axis along the surface of the crystal.

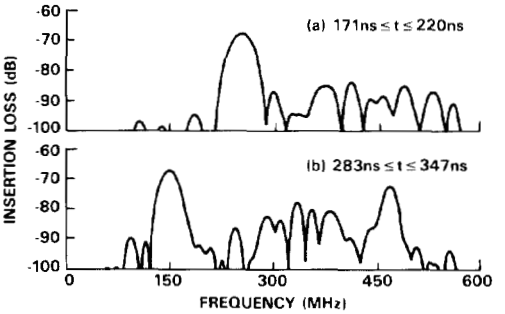

Fig. 10. Fourier transforms of portions of the time domain data of Fig. 9. Before taking the transforms, time domain data was nulled everywhere except in regions specified on each plot.

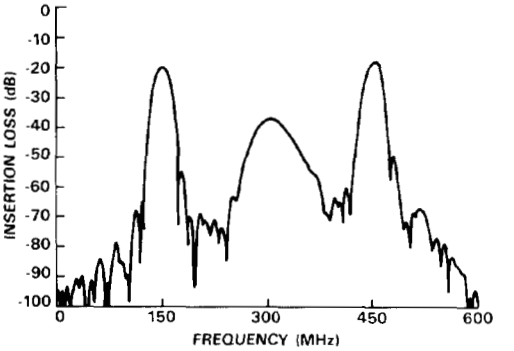

Fig. 11. SAW filter insertion loss data after Fourier transforming to time domain, time gating to include only the region from 266.8 ns ≤ t ≤ 413.2 ns, and Fourier transforming back to the frequency domain.

Thus, the frequency domain data confirm the fact that the only remaining modes after sandblasting are the on-axis acoustic modes that skim along the surface of the crystal.

The surface wave insertion loss at 150 MHz was 21 dB. Fig. 10 shows a residual signal left by the on-axis slow shear wave that is 47 dB down from the Rayleigh wave response. Comparison of Fig. 10 to the SAW response at other frequencies shows that the first sidelobe of the Rayleigh response is ~30 dB above the residue shown in Fig. 10 and the second SAW sidelobes is ~22 dB above the acoustic residue of Fig. 10.

VII. Waveform Processing

The preceding analysis of the physical mechanisms for acoustic bulk wave propagation in 128°$LiNbO_3$ has lead to the definition of a SAW filter analysis procedure in which the interfering bulk waves can be eliminated from consideration. Fig. 4 shows the time domain response of the SAW filter without sandblasting. Counting the crosstalk term there are five responses in the impulse response. Only one pulse, the one at 320 ns is coincident with the Rayleigh wave impulse response. If the impulse response is windowed to exclude signals away from the Rayleigh response and then Fourier transformed, all that can appear in the frequency domain response are the bulk-wave responses shown in Fig. 5(c) and the Rayleigh-wave responses in the SAW passband at 150 MHz are at a relatively low level. The majority of the response due to the time response. Fig. 5(c) shows that those frequency responses in the SAW passband at 150 MHz are at a relatively low level. The majority of the response due to the time response at 320 ns occurs at much higher frequencies. Thus, one can perform Fourier transform operations on measured data from unsandblasted devices and convert the data to a form which more nearly represents the Rayleigh wave alone. Such a plot is illustrated in Fig. 11. By comparing Fig. 5(c) with Fig. 11, one can see that Fig. 11 is a summation of Fig. 5(c) with the Rayleigh-wave response. Comparing the levels, one can see that the center frequency spurious level is down 48 dB and that the first two sidelobes have bulk wave interference at -25 and -10 dB, respectively, relative to the SAW sidelobe level.

The majority of the energy associated with the bulk waves at 150 MHz will be both amplitude and phase correlated to the SAW response because it is an on-axis mode and not influenced by the backside of the crystal. Thus, its frequency response will not vary with substrate geometry. Only those portions of the acoustic response associated with reflection from the backside of the crystal will vary with crystal backside treatment and with packaging variations. Accordingly, it may be that a "scrubbed" response which includes only the Rayleigh mode and those modes traveling Path 0 is the desired S_{21} representation. In the current filter, after waveform processing, a small portion of the Path 1 signal remained in-band of the Rayleigh response. Those portions of the time domain response associated with Path 1 of Fig. 1 could in fact be separated from the SAW impulse response by adjustment of substrate geometry. In that case the only signals that could not be time resolved from the SAW response would be the on-axis modes. The potential thus exists to conduct IDT analysis using transformed versions of measurements made on unsandblasted devices. In many cases, these "scrubbed" responses can be sufficiently undistorted to allow study of just SAW excitation by specific features in an IDT.

VII. Conclusion

We have illustrated in the case of SAW IDT's on $(YXl)128°$-$LiNbO_3$ the several forms of bulk wave energy transport. Each mode of energy transport has been delineated in both time and frequency, showing that both longitudinal and slow shear wave signals travel along the top surface of the crystal. It has also been shown that a substantial portion of the bulk wave interference arises from energy transport paths in which the signals bounce off the backside of the crystal. Both slow shear and longitudinal waves can travel paths in which they execute one bounce off the backside of the crystal and in each case scatter into an upward traveling version of the incident mode. Additionally, a one-bounce mode conversion process was identified. Within the dynamic range of the experimental procedures reported here, no multiple bounces were observed in the filter characteristics.

Perhaps the most significant finding of this work is that the terminal response of the SAW filter can be "scrubbed" to achieve frequency responses more representative of single-mode transport. While this procedure will not help the filter designer create a filter which has no bulk mode distortion in its characteristics, this approach is of great value to the analyst attempting to quantify the interaction between the IDT and a single mode. The terminal properties, of course, are a superposition of the IDT's interaction with each mode. This technique can also be used to advantage as a yield-enhancing and time-saving step in the design of a SAW filter in which one

knows that the final filter will not have certain of the bulk mode responses in its terminal properties. Rather than go through the fabrication steps necessary to eliminate these bulk responses from the terminal properties, prototype filters can be examined at an earlier stage of fabrication when the bulk modes are still present in S_{21} and simply have those responses scrubbed from the network analyzer measurements.

REFERENCES

[1] R. F. Milsom, N.H.C. Reilly, and M. Redwood, "Analysis of generation and detection of surface and bulk acoustic waves by interdigital transducers," *IEEE Trans. Sonics Ultrason.*, vol. SU-24, no. 3, pp. 147–166, May 1977.

[2] R. S. Wagers, "Plate modes in surface acoustic wave devices," in *Physical Acoustics*, Vol. 13, W. P. Mason and R. N. Thurston, Eds. New York: Academic Press, 1977, pp. 49–78.

[3] K. Shibayama, K. Yamanouchi, H. Sato, and T. Meguro, "Optimum cut for rotated Y-cut $LiNbO_3$ crystal used as the substrate of acoustic-surface-wave filters," *Proc. IEEE*, vol. 64, no. 5, pp. 595–597, May 1976.

[4] R. F. Milsom, R. J. Murray, I. Flinn, and M. Redwood, "New orientation of lithium niobate for low bulk-wave degradation of SAW filter stopband," in *Proc. IEEE Ultrason. Symp.*, Chicago, IL, Oct. 1981, pp. 299–304.

[5] R. F. Milsom, R. J. Murray, and I. Flinn, "Ultra low bulk orientation of lithium niobate for SAW TV filters," *Electron. Lett.*, vol. 17, no. 2, pp. 89–91, Jan. 22, 1981.

[6] K. Yashiro and N. Goto, "Analysis of generation of acoustic waves on the surface of a semi-infinite piezoelectric solid," *IEEE Trans. Sonics Ultrason.*, vol. SU-25, no. 3, pp. 146–153, May 1978.

[7] R. S. Wagers and R. W. Cohn, "Development of SAW filter perturbation techniques," in *Proc. IEEE Ultrason. Symp.*, Atlanta, GA, Oct. 1983, pp. 5–10.

[8] J. R. Klauder, A. C. Price, S. Darlington, and W. J. Albersheim, "The theory and design of chirp radars," *Bell Syst. Tech. J.*, vol. 34, no. 4, July 1960, pp. 745–809.

[9] R. S. Wagers, "Effect of finite aperture on spurious mode levels in acoustic surface wave filters," *IEEE Trans. Sonics Ultrason.*, vol. SU-22, no. 5, pp. 375–379, Sept. 1975.

[10] —, "Spurious acoustic responses in SAW devices," *Proc. IEEE*, vol. 64, no. 5, pp. 699–702, May 1976.

[11] E. O. Brigham, *The Fast Fourier Transform*. Englewood Cliffs, NJ: Prentice-Hall, 1974, pp. 91–109.

Robert S. Wagers (S'67–M'75–SM'78–F'84) was born in Covington, KY, on January 25, 1943. He received the B.S.E.E. (1966) and M.S.E.E. (1967) degrees from Arizona State University, Tempe, and the Ph.D. degree (1972) from Stanford University, Stanford, CA.

He is Manager of the Surface Acoustic Wave Devices branch of the Central Research Laboratories of Texas Instruments Incorporated. His current research interests involve the integration of surface acoustic waves with semiconducting devices. Previously at Texas Instruments he has been Manager of the CCD Imaging Systems branch (1977–1978) and a Member of the Technical Staff (1972–1976). As a Staff Member he conducted research on acoustic signal processing. His responsibilities have included the investigation of acoustic ridge waveguides, development of synthesis techniques for surface acoustic wave filters and modeling of second-order distortion effects in surface acoustic wave devices. Prior to joining Texas Instruments, Dr. Wagers held positions as a Research Assistant at Stanford University where he investigated the excitation of surface acoustic waves on nonpiezoelectric substrates (1970–1972), and nonlinear warm plasma instabilities (1967–1970). During 1966 and 1967, as a Rhodes Scholar at Oxford University, England, he worked on accelerator structures for X-band pulse compressors. In the fall of 1976, Dr. Wagers was Assistant Professor of Electrical Engineering at Princeton University. He has 50 publications and nine U.S. patents to his credit.

Dr. Wagers is an Associate Editor for SAW devices of the IEEE TRANSACTIONS ON SONICS AND ULTRASONICS, member of the Sonics and Ultrasonics Group (GSU) Awards Committee, and member of the GSU AdCom. He received the IEEE GSU Best Paper Award in 1976.

Robert Warren Cohn (M'79) was born in Cleveland, OH, July 21, 1953. He received the B.S. and M.S. degrees in electrical engineering from the University of Kansas, Lawrence, in 1978 and 1982, respectively. He also holds the B.A. degree in English from the University of Kansas (1975).

Mr. Cohn is a Member of the Technical Staff of the Central Research Laboratories of Texas Instruments. In his current research he is investigating empirical methods for the optimization of SAW filter performance. From 1978 to 1983 he worked in the Equipment Group of Texas Instruments where he was engaged in SAW device and microwave hybrid design and development.